NASA TECHNICAL MEMORANDUM

NASA TM X-2161

NASA TM X-2161

OPERATING CHARACTERISTICS OF THE PRIMARY FLOW LOOP OF A CONCEPTUAL NUCLEAR BRAYTON SPACE POWERPLANT

by George E. Turney, Arthur W. Kieffer, and Edward J. Petrik

Lewis Research Center
Cleveland, Ohio 44135

NATIONAL AERONAUTICS AND SPACE ADMINISTRATION • WASHINGTON, D. C. • MARCH 1971

1. Report No.	2. Government Accession No.	3. Recipient's Catalog No.
NASA TM X-2161		

4. Title and Subtitle	5. Report Date
OPERATING CHARACTERISTICS OF THE PRIMARY FLOW LOOP OF A CONCEPTUAL NUCLEAR BRAYTON SPACE POWERPLANT	March 1971
	6. Performing Organization Code
7. Author(s)	8. Performing Organization Report No.
George E. Turney, Arthur W. Kieffer, and Edward J. Petrik	E-5903
	10. Work Unit No. 120-27
9. Performing Organization Name and Address	11. Contract or Grant No.
Lewis Research Center National Aeronautics and Space Administration Cleveland, Ohio 44135	
	13. Type of Report and Period Covered
12. Sponsoring Agency Name and Address	Technical Memorandum
National Aeronautics and Space Administration Washington, D.C. 20546	14. Sponsoring Agency Code

15. Supplementary Notes

16. Abstract

An analytical study was made of the steady-state and transient operating characteristics of the lithium cooled primary flow loop of a conceptual nuclear Brayton space powerplant. From the system investigation, it was determined that (1) the steady-state power of the reactor varies linearly with (a) the inserted reactivity and (b) the flow rate of inert gas in the Brayton power conversion loop (2) the flow rate of lithium in the primary loop has a small effect on the reactor steady-state power. The transient changes in the reactor power and temperature of the primary loop were determined for step input disturbances in (1) inserted reactivity, (2) lithium flow rate in the primary loop, and (3) inert-gas flow rate in the Brayton power conversion loop. The response of the system to these step changes can be characterized as stable and highly damped.

17. Key Words (Suggested by Author(s))	18. Distribution Statement
Nuclear space power reactor Operating characteristics Steady-state and transient	Unclassified - unlimited

19. Security Classif. (of this report)	20. Security Classif. (of this page)	21. No. of Pages	22. Price*
Unclassified	Unclassified	37	$3.00

*For sale by the National Technical Information Service, Springfield, Virginia 22151

OPERATING CHARACTERISTICS OF THE PRIMARY FLOW LOOP OF A CONCEPTUAL NUCLEAR BRAYTON SPACE POWERPLANT

by George E. Turney, Arthur W. Kieffer, and Edward J. Petrik

Lewis Research Center

SUMMARY

An analytical investigation was made of the steady-state and transient operating characteristics of the lithium cooled primary flow loop of a conceptual nuclear Brayton space powerplant. In this conceptual system, the lithium cooled primary loop is coupled directly to an inert-gas power conversion loop by a heat exchanger. The heat source for this conceptual powerplant is a 2.17-megawatt fast-spectrum reactor.

From this system investigation, it was determined that: (1) the reactor steady-state power varies linearly with the inserted reactivity, (2) the reactor steady-state power varies linearly with the inert-gas flow rate in the power conversion loop, and (3) the flow rate of lithium in the primary loop has a small effect on the reactor steady-state power.

The transient changes in the reactor power and temperatures of the primary loop were determined for step input disturbances in (1) inserted reactivity, (2) lithium flow rate, and (3) inert-gas flow rate. The response of the system to these step changes can be characterized as stable and highly damped. For reactivity step changes ranging from 5 to 30 cents, the reactor power settling time was approximately constant and equal to about 275 seconds.

The transient response of the system was also investigated with Doppler reactivity coefficients which were negative, zero, and positive in value. In general, the response of the system did not change appreciably with the different values of Doppler coefficient used in the investigation.

INTRODUCTION

The electric power requirements for our nation's furture space programs will continue to increase. In view of this, the Lewis Research Center has been working on a

technology program aimed at the design of an advanced, high-powered, nuclear Brayton space powerplant.

The heat source being considered for this advanced space powerplant is a compact, fast-spectrum, nuclear reactor. The design power output of the reactor is 2.17 megawatts thermal (ref. 1); and the design operating lifetime for the reactor and powerplant has been set at 50 000 hours.

In this conceptual system, the heat generated by the reactor is removed by liquid lithium which circulates continuously through a closed primary flow loop. The primary loop is coupled directly to a Brayton inert-gas power conversion loop by a heat exchanger.

An analytical study was made of the operating characteristics of the primary flow loop of this conceptual space powerplant. The objectives of the study were (1) to investigate the steady-state operation of the primary loop at different off-design operating conditions, (2) to determine the transient response of the primary loop to step disturbances (forced perturbations) in reactivity, lithium flow rate in the primary loop, and inert-gas flow rate in the Brayton power conversion loop, and (3) to investigate the effect of the Doppler reactivity feedback on the transient response characteristics of the system.

The study was made using an analog computer. The results of the study along with descriptions of the system equations and the models used to represent the reactor and heat exchanger are presented in this report.

SYSTEM DESCRIPTION

A simplified diagram of the conceptual nuclear Brayton space powerplant is shown in figure 1. This sytem, in its present design configuration, has a single lithium cooled primary loop, one or more complete inert-gas power conversion loops, and a main radiator loop for waste heat rejection. (The design configuration shown in fig. 1 and described here is preliminary. Studies are currently being made to arrive at a final design configuration for the system.)

The path of coolant flow in each of the loops is indicated in figure 1. During normal operation, the heat gained by the lithium as it flows through the reactor is transferred to the gas power conversion loop by the heat-source heat exchanger. The heated inert-gas is then expanded through a turbine. The work produced by the turbine drives a compressor and an electrical alternator. The turbine exhaust gas is cooled as it flows first through the recuperator and then through the waste heat exchanger.

For this preliminary study, the working fluid in the power conversion loop is assumed to be argon gas. The feedback effects of the gas power conversion loop and main

radiator loop were not considered in this study. Instead, the power conversion loop was considered as an open loop, and the temperature of the argon gas entering the heat-source heat exchanger was assumed constant at 1560° R (867 K). The design point operating conditions for this space power system relevant to this study are listed in table I.

ANALYSIS

In order to analyze the operating characteristics of the primary loop on the analog computer, models were formulated to represent the reactor core and the heat-source heat exchanger. In this section, we describe these models and also the equations used in the analysis.

Reactor Core

The present reactor core design for this space powerplant has 253 cylindrical fuel pins, each with a diameter of 3/4 inch (1.905 cm) and a length of 14.8 inches (37.6 cm). The fuel pins are made of uranium nitride and are clad with a tantalum alloy and a tungsten liner. The interior of each fuel pin has a central void of 0.202 inch (0.513 cm) diameter. The core assembly is cooled by lithium which flows through annular passages formed by the outside surfaces of the fuel pins and the inside surfaces of concentric tantalum tubes which surround the fuel pins. The inside diameter of the surrounding tantalum tubes is 0.830 inch (2.11 cm).

Reactor power is regulated by six control drums which, when rotated, move fuel (or a tantalum neutron absorber) in or out of the core region. Figure 2 shows a cutaway view of the reactor core design for this space power system. A detailed description of this reactor design is given in reference 1.

The analog model used to represent the core consists of a single fuel pin with the composition and dimensions stated previously. For calculation purposes, the single fuel pin model of the core was divided into three axial segments of equal length. Each segment, consisting of fuel, cladding, and lithium coolant is described by a set of equations. A sketch of the single fuel pin model of the core is shown in figure 3.

Reactor core models with other than three segments were also investigated on the analog computer and it was determined that the three segment model provided a reasonably accurate representation of the reactor core.

Core Analytical Equations

Core kinetics. - The thermal power generated by the reactor was determined from the following equation (ref. 2):

$$\frac{d\dot{Q}}{dt} = \left(\frac{\delta k - \beta}{l^*}\right)\dot{Q} + \sum_{i=1}^{6} \lambda_i D_i \tag{1}$$

(All symbols are defined in appendix A.) As indicated by equation (1), six delayed neutron groups were considered.

The rate of change in concentration of the delayed neutron precursors (ref. 2) is given by

$$\frac{dD_i}{dt} = \frac{\beta_i}{l^*}\dot{Q} - \lambda_i D_i \tag{2}$$

The decay constants and yield fractions of the precursors for the six delayed neutron groups and the prompt neutron generation time are listed in table II. The values in table II were obtained from reference 1.

As a point of interest, the magnitude of the term $d\dot{Q}/dt$ in equation (1) is negligible in comparison to the other terms in this equation. Because of this, we assumed in our analysis that the left side of equation (1) vanishes. This simplification of equation (1) is similar to the "promt jump" approximation described by Ash (ref. 3).

Reactivity. - For the reactor analysis, the power coefficient of reactivity included three separate feedback effects. They are (1) the Doppler coefficient for the reactor fuel and cladding, (2) the core geometric expansion temperature coefficient, and (3) the density temperature coefficient for the lithium coolant. A block diagram of the core with these three feedback loops is depicted in figure 4.

The reactivity feedbacks due to the Doppler effect, the core expansion, and the lithium density change were calculated from the following expressions:

$$\frac{d(\delta k_D)}{dT} = \frac{d(\delta k_{D,F})}{dT_{F,av}} + \frac{d(\delta k_{D,K})}{dT_{K,av}} = \frac{2.17\times10^{-4}}{T_{F,av}} - 6.465\times10^{-4}T_{K,av}^{-0.8} \tag{3}$$

$$\frac{d(\delta k_E)}{dT_{L,av}} = -5.69\times10^{-6} \tag{4}$$

$$\frac{d(\delta k_\rho)}{dT_{L,av}} = -1.627\times10^{-6} \tag{5}$$

The feedback coefficient for the core geometric expansion (eq. (4)) is based on the average lithium temperature in the core. This is a reasonable approximation since the core average temperature is near the average lithium temperature.

The terms $T_{F,av}$, $T_{K,av}$, and $T_{L,av}$ in equations (3), (4), and (5) represent the average temperatures of the fuel, cladding, and lithium in the core, respectively. These average temperatures were determined by weighting the respective temperatures in each axial segment of the core in proportion to the design axial power distribution.

The axial power distribution at the design operating point was determined from a calculation made with the TDSN neutron transport code (ref. 4). The shape of the axial power distribution at the design point resembles a chopped cosine. This axial power distribution was assumed to be the same at all thermal power levels. The power in the three axial segments of the core was distributed such that about 39.0 percent was produced in the middle segment (segment 2) and about 30.5 percent was produced in each of the other two segments (segments 1 and 3).

Hence, for the feedback terms, the average temperatures of the fuel, cladding, and lithium in the core were determined from the segment average temperatures as follows:

$$T_{F,av} = 0.39\,\overline{T}_{F(seg\ 2)} + 0.305\left[\overline{T}_{F(seg\ 1)} + \overline{T}_{F(seg\ 3)}\right] \tag{6}$$

$$T_{K,av} = 0.39\,\overline{T}_{K(seg\ 2)} + 0.305\left[\overline{T}_{K(seg\ 1)} + \overline{T}_{K(seg\ 3)}\right] \tag{7}$$

$$T_{L,av} = 0.39\,\overline{T}_{L(seg\ 2)} + 0.305\left[\overline{T}_{L(seg\ 1)} + \overline{T}_{L(seg\ 3)}\right] \tag{8}$$

The design values of average fuel, clad, and lithium temperatures in the core along with the values of the feedback coefficients at the design temperatures are listed in table III.

Core heat transfer. - Heat-transfer equations for the core were derived based on the single fuel pin model shown in figure 3. The average fuel temperature of each segment of the core was computed from the following equation:

$$\frac{d\overline{T}_F}{dt} = \frac{k_{F,av}A_{m,F}}{\rho_F V_F C_{p,F}} \frac{\left(\overline{T}_K - \overline{T}_F\right)}{\Delta r_F} + \frac{f\dot{Q}}{\rho_F V_F C_{p,F}} \tag{9}$$

And the cladding temperature in each segment of the core was determined from the equation

$$\frac{d\overline{T}_K}{dt} = \frac{k_{K,av} A_{m,K}}{\rho_K V_K C_{p,K}} \frac{(\overline{T}_F - \overline{T}_K)}{\Delta r_K} + \frac{h_{L,c} S_c (\overline{T}_L - \overline{T}_K)}{\rho_K V_K C_{p,K}} \tag{10}$$

The lithium temperature in each axial core segment was computed from the expression

$$\frac{d\overline{T}_{L,c}}{dt} = \left(\frac{\dot{\omega}_L}{\rho_L A_L}\right) \frac{\Delta T_{L,c}}{\Delta X_c} + \left(\frac{h_{L,c} S_c}{\rho_L V_L C_{p,L}}\right) (\overline{T}_L - \overline{T}_K) \tag{11}$$

The average lithium temperature in each core segment was assumed equal to the arithmetic mean of the lithium temperature at the segment inlet and outlet. Hence, the lithium temperature at the outlet of a core segment is equal to twice the average lithium temperature minus the lithium temperature at the segment inlet; that is, $T_{L,out} = 2\overline{T}_L - T_{L,in}$.

Heat-Source Heat Exchanger

In this preliminary study, a counterflow shell-and-tube-type configuration was assumed for the heat-source heat exchanger. This heat exchanger has 331 tantalum flow tubes; the tubes were assumed to have an inside diameter of 3/4 inch (1.905 cm), a wall thickness of 0.05 inch (0.127 cm), and a length of approximately 8 feet (2.44 m).

Argon gas flows inside the tubes and lithium flows countercurrently in the shell. The tubes in this heat exchanger configuration are arranged in a hexagonal cross-sectional array, with a centerline-to-centerline spacing between tubes equal to 1.01 inches (2.565 cm).

The heat exchanger just described should not be considered as a design configuration. Rather it is a conceptual configuration established for this study, which is capable of transferring the heat load from the primary loop to the gas power conversion loop.

The analog computer model for this heat exchanger is a single tube, made of tantalum, with argon flowing inside the tube and lithium flowing countercurrently on the outside. Figure 5 is a sketch of the analog model used to represent the heat exchanger. As indicated in this figure, the single tube model is made up of three axial segments of equal length.

The length of the single tube model is the same as that of the shell-and-tube heat exchanger assembly. And by the principle of similarity, it can be shown that the single

tube model, with the cross-sectional dimensions shown in figure 5, gives a reasonably accurate representation of the shell-and-tube heat exchanger assembly.

Heat Exchanger Equations

The heat-transfer equations for the heat-source heat exchanger were derived based on the single tube model shown in figure 5. In the derivation of the equations, the thermal resistance to heat transfer by conduction across the wall of the heat exchanger was determined to be relatively small, and was therefore neglected.

The average temperature of lithium in each heat exchanger segment was determined from the equation

$$\frac{d\overline{T}_{L,HX}}{dt} = \frac{\dot{\omega}_L}{\rho_L A_L}\frac{\Delta T_{L,HX}}{\Delta X_{HX}} + \frac{h_{L,HX} S_{L,HX}}{\rho_L V_L C_{PL}}\left(\overline{T}_{W,HX} - \overline{T}_{L,HX}\right) \tag{12}$$

And the average wall temperature for each segment of the heat exchanger was computed from the equation

$$\frac{d\overline{T}_{W,HX}}{dt} = \frac{h_{L,HX} S_{L,HX}}{\rho_W V_W C_{p,W}}\left(\overline{T}_{L,HX} - \overline{T}_{W,HX}\right) + \frac{h_g S_{g,HX}}{\rho_W V_W C_{p,W}}\left(\overline{T}_g - \overline{T}_{W,HX}\right) \tag{13}$$

The average temperature of the argon gas in each axial segment of the heat exchanger was computed from the expression

$$\frac{d\overline{T}_g}{dt} = \frac{\dot{\omega}_g}{A_g \rho_g}\frac{\Delta T_{g,HX}}{\Delta X_{HX}} + \frac{h_g S_{g,HX}}{\rho_g V_g C_{p,g}}\left(\overline{T}_{W,HX} - \overline{T}_g\right) \tag{14}$$

Expressions were developed for use on the analog to relate (1) the average temperature of lithium in a heat exchanger segment to the lithium temperature change across the segment, and (2) the average temperature of argon in a heat exchanger segment to the argon temperature change across the segment. These expressions were obtained from steady-state solutions of the heat exchanger equations at different operating conditions.

Heat-Transfer Coefficients

The average lithium heat-transfer coefficient in each of the three longitudinal segments of the core was determined from the following equation (ref. 5):

$$Nu_{L,c} = 5.591 + 4.595\times10^{-4}(Re_{L,c})^{0.7998} \tag{15}$$

The average lithium heat-transfer coefficient in each of the three longitudinal segments of the heat exchanger was computed from the following equation (ref. 6):

$$Nu_{L,HX} = 8(Pe_{L,HX})^{0.6}\left[\frac{D_{L,HX}}{L_{HX}} + 0.027\left(\frac{s}{d} - 1.10\right)\right]^{0.46} \tag{16}$$

An appropriate average value of $D_{L,HX}/L_{HX}$ was used in equation (16) to calculate the average lithium heat-transfer coefficient in each segment of the heat exchanger.

The average argon heat-transfer coefficient in each segment of the heat exchanger was calculated from the Dittus-Boelter expression (ref. 7); that is,

$$Nu_g = 0.023(Re_g)^{0.8}(Pr_g)^{0.4} \tag{17}$$

Representation of Transport Delay

In a closed loop system, the loop transport delay (or delay time) is defined as the time required for the coolant to traverse the loop. In the primary loop of the nuclear Brayton space powerplant, nearly all of the loop transport delay occurs in the heat-source heat exchanger. Consequently, only the transport delay in the heat exchanger was considered.

In this study, the loop transport delay was simulated on the analog computer by a fourth-order cut-product approximation described in reference 8. Because of the transport delay, the fluid temperatures at the outlet of each of the three heat exchanger segments were delayed by one-third of the loop transport time before entering the next heat exchanger segment. At the design value of lithium flow rate, the loop transport delay is about 10 seconds. Hence, at the design flow rate of lithium, a change in the lithium temperature at the reactor outlet goes unnoticed at the reactor inlet for a time period of about 10 seconds.

It should be recognized that the value of the transport delay just stated is a characteristic of the heat exchanger configuration used in this study.

RESULTS AND DISCUSSION

The equations listed in the ANALYSIS section of this report were systematically programmed and analyzed on an analog computer.

From this study, information was obtained on (1) the steady-state operating characteristics of the primary flow loop, (2) the transient response characteristics of the primary loop, and (3) the effect of the Doppler reactivity feedback on the transient response of the primary loop.

This information is described in the paragraphs which follow.

Steady-State Operating Characteristics

The steady-state results of the analog computer study are presented in figure 6 to 11. These figures represent a map of the steady-state operating points of the primary loop at various percentages of the design point operating conditions. In particular, the figures indicate how the steady-state operating variables (i.e., reactor power, fuel temperatures, and lithium coolant temperatures) are affected by (1) inserted reactivity, (2) lithium flow rate in the primary loop, and (3) argon gas flow rate in the power conversion loop. A discussion of the steady-state operating data are presented below.

Figure 6 shows the reactor thermal power as a function of inserted reactivity. This curve is based on the assumption that the flow rates in the primary loop and gas power conversion loop are at their respective design point values. (The design point operating values are given in table I).

At steady-state, the inserted reactivity is exactly counterbalanced by the feedback terms. Hence, each point on the curve in figure 6 represents a condition for which inserted reactivity is exactly counter-balanced by the feedback; and the effective multiplication factor k_{eff} is one.

The feedbacks used to generate the data in figure 6 were computed from equations (3), (4), and (5). Based on these feedback values, figure 6 shows that the reactor steady-state power varies linearly with reactivity insertion. And the change in reactor steady-state power is about 12 percent for each 10 cents of reactivity insertion (1 dollar = 100 cents = 0.0066 reactivity).

Normally, the reactor thermal power is regulated by changing the position of the control drums. But reactor power is also affected by the flow rate of argon gas in the

power conversion loop. (The argon flow rate affects the rate of heat removal from the primary loop; this, in turn, causes a change in reactor temperature. And because of the feedbacks, the reactor power also changes.) Figure 7 shows reactor steady-state power as a function of argon flow rate. This figure shows reactor power changes significantly with argon flow rate. A 10 percent change in the argon flow rate causes about a 9 percent change in reactor steady-state power. The change in reactor power is directly proportional to argon flow rate.

In contrast to the large effect which argon flow rate has on reactor steady-state power, the lithium flow rate has a relatively small effect. Figure 8 is a plot of reactor steady-state power against lithium flow rate with argon flow rate as a parameter.

For lithium flow rates greater than 50 percent of the design value, the reactor power is nearly independent of lithium flow rate. Figure 8 shows that with the system initially at its design point, an increase of 15 percent in lithium flow rate causes the reactor steady-state power to increase by about 0.05 percent. This behavior can be explained by the fact that the overall heat-transfer coefficient of the heat-source heat exchanger is nearly independent of the lithium flow rate, particularly at low values of argon flow rate. As a consequence, the average temperatures of the fuel, clad, and lithium is the reactor (i.e., $T_{F,av}$, $T_{K,av}$, and $T_{L,av}$) are nearly constant over a wide range of lithium flow rates. Only at the lower lithium flow rates does the average reactor temperature increase. And because of the temperature reactivity feedbacks, the reactor thermal power decreases.

Figure 9 shows the steady-state average fuel temperatures of fuel segments 1, 2, and 3 against lithium flow rate with argon flow rate as a parameter. At a particular value of argon flow rate, the average steady-state temperatures of fuel segments 1 and 3 vary considerably with lithium flow rate. But the average steady-state temperature of fuel segment 2 is nearly constant and independent of lithium flow rate.

In spite of the variation of the fuel temperatures of segments 1 and 3 with lithium flow rate, the average temperature of the fuel (i.e., $T_{F,av}$ in eq. (6)) is nearly constant for a particular argon flow rate, provided the lithium flow rate is greater than about 50 percent of the design value.

The steady-state temperatures of lithium at the core inlet and core outlet are shown as a function of lithium flow rate in figure 10. The curves in figure 10 are based on the assumption that the argon flow rate is at its design value. As shown in figure 10, the lithium temperature at the entrance to the core decreases as the lithium flow rate decreases. This effect originates in the heat-source heat exchanger and is the result of a longer dwell time of lithium. More cooling of the lithium takes place in the heat exchanger; consequently, the lithium temperature at the heat exchanger exit decreases. (The lithium temperature at the heat exchanger exit is equivalent to the lithium temperature at the core inlet.)

Similarly, because the lithium dwell time in the core is longer, the lithium temperature at the core outlet increases as the lithium flow rate decreases.

Figure 11 shows the steady-state lithium temperatures at the inlet and outlet of the core as a function of argon flow rate. The data in figure 11 are based on the assumption that the lithium flow is at its design value. Comparing figure 11 with figure 10 reveals that variations in lithium and argon flow rates have opposing effects on the lithium temperatures. In figure 11, the lithium temperature at the core inlet increases as argon flow decreases. This is because a reduction in argon flow lowers the heat-transfer rate in the heat exchanger. And this causes the average lithium temperature to increase at most locations in the primary loop. Because of an increase in temperature throughout most of the core, the reactivity feedbacks cause the power to be reduced. A reduction in power thus causes less temperature rise of the lithium through the core; and this explains the subsequent decrease in lithium temperature at the core outlet.

Transient Operating Characteristics

The transient operating characteristics of the primary loop were investigated with the analog computer by putting step disturbances into the system. The disturbances were imposed on each of the following system variables:

(1) Reactivity

(2) Lithium flow rate in the primary loop

(3) Argon flow rate in the power conversion loop

The reactivity feedbacks used for this portion of the study were computed from equations (3), (4), and (5). In the following paragraphs, we describe the response of the system primary loop to each of the three types of step input disturbances.

Step changes in reactivity. - With the system operating at its steady-state design point, step changes were made in reactivity. Reactivity steps of 5, 10, 20, and 30 cents were used.

The thermal power output of the reactor, corresponding to these reactivity step changes, is shown as a function of time in figure 12. (Time zero coincides with the step input in reactivity.) For each of the reactivity steps shown in figure 12, the reactor power reaches a peak or maximum value in the time span from 25 to 50 seconds.

Although reactor power varies significantly with the reactivity step size, the "settling time" corresponding to each reactivity step is approximately the same and is equal to about 275 seconds. (The reactor power settling time, as used here, is defined as the time required for the power to reach and thereafter remain within 5 percent of the steady-state change in reactor power.)

The average temperatures of the fuel in segments 1, 2, and 3 of the core are shown against time in figure 13. An interesting feature of the data in figure 13 is that, in each segment of the core, the ratio of the fuel peak temperature change to steady-state temperature change is nearly constant for all values of reactivity step change shown. The approximate ratios of fuel peak temperature change to steady-state temperature change for segments 1, 2, and 3 of the core are 1.28, 1.36, and 1.39, respectively. The fact that these ratios are nearly constant signifies that, for the reactivity step sizes investigated, the percent overshoot in fuel temperature in each axial segment of the core is essentially constant.

The lithium temperatures at the core inlet and core outlet are shown as a function of time in figure 14. A comparison of figures 14(a) and (b) shows that the lithium temperature at the core outlet (fig. 14(b)) changes immediately following a reactivity step change. But the lithium temperature at the core inlet (fig. 14(a)) remains unchanged for about 10 seconds after the reactivity step. This lag in response is caused by the transport delay in the heat exchanger. (See the section Representation of Transport Delay.)

An inspection of the curves in figures 14(a) and (b) shows that the ratios of peak lithium temperature change to final steady-state lithium temperature change at both the core inlet and core outlet are nearly constant and equal to about 1.25. Hence, for the range of reactivity steps used, the percent over-shoot in the lithium temperatures is essentially constant and equal to 25 percent.

The temperature of argon at the heat exchanger outlet is shown against time in figure 15. For each value of reactivity step change, the ratio of argon peak temperature change to final steady-state temperature change is approximately equal to 1.24. And for the range of reactivity steps shown in figure 15, the percent overshoot in argon temperature is about 24 percent.

Figure 16 shows the transient peak and steady-state values of reactor power, lithium temperature rise across the core, and fuel section temperatures as a function of reactivity step insertion. The transient peaks in figure 16 represent the maximum values which the variables reach following a step change in reactivity.

A step change represents the most severe type of input disturbance. Therefore, it is expected that, for other types of reactivity input disturbances, the maximum values reached by the variables will remain below the transient peak values shown in figure 16.

Step change in lithium flow rate. - With the system initially at steady-state design conditions, a step increase of 15 percent was made in the lithium flow rate. The response of the system to this step change is shown in figure 17. Time zero in this figure corresponds to the initiation of this step change.

The immediate effect of this disturbance is an increase in the lithium velocity through the reactor and heat exchanger. The velocity increase has little effect on the lithium heat-transfer coefficient. But it does reduce the dwell time of lithium in the

reactor and heat exchanger. As a result, there is a smaller lithium temperature change across both the reactor core and heat exchanger.

The temperature of lithium at the reactor inlet and reactor outlet are shown against time in figures 17(a) and (b), respectively. Immediately following the step change in lithium flow rate, the lithium temperature at the reactor inlet increases. And the lithium temperature at the reactor outlet decreases. This temperature behavior of lithium is caused by the interaction (or coupling) between the core and heat exchanger. After about 30 seconds, most of temperature transients die out. And the lithium temperature approach their final steady-state values.

The fuel temperatures in the three segments of the core, following the step change in lithium flow rate, are shown against time in figures 17(c), (d), and (e). The largest change in fuel temperature takes place in segment 3 (fig. 17(e)). This maximum change (at times equals about 4 sec) is only about -8° R (-4.5 K).

Figure 17(f) shows the reactor thermal power against time after the step change in lithium flow rate. Because of the negative temperature feedbacks, the reactor power responds to oppose the change in the lithium temperatures and fuel temperatures. The maximum variation in reactor power is small (about 1.2 percent). Its effect on the system is therefore negligible.

Figure 17(g) shows the temperature of argon at the heat exchanger outlet against time after the step change in lithium flow rate. The maximum change in argon temperature is about 2° R (1.1 K), and the final steady-state change is only about 0.35° R (0.18 K).

From the preceding discussion, it is apparent that changes in lithium flow rate have a relatively small effect on the final steady-state conditions in the system primary loop.

Step change in argon flow rate. - At time zero, with the system operating at design conditions, a step increase of 15 percent was made in the argon flow rate. The subsequent system response to this step change is shown in figure 18.

The increase in argon flow rate directly affects the system in two ways. First, it reduces the dwell time of the argon gas in the heat exchanger, and second, it improves the gas side heat-transfer coefficient in the heat exchanger.

Figure 18(a) shows the argon temperature at the heat exchanger outlet against time. For the first 50 seconds after the argon flow rate change, the argon temperature at the heat exchanger outlet decreases. This initial decrease occurs because the dwell time of the argon gas in the heat exchanger is reduced. After the first 50 seconds, the argon temperature at the heat exchanger outlet increases and approaches a final steady-state value.

The lithium temperatures at the core inlet and core outlet are shown against time in figures 18(b) and (c), respectively. These temperatures decrease initially because of an increase in the heat-transfer rate to the gas loop. The increased heat-transfer rate is

caused by an increase in the gas side heat-transfer coefficient and by a lower gas temperature in the heat exchanger. The lithium temperatures shown in figures 18(b) and (c) eventually increase and approach their final steady-state values. The eventual increase in these lithium temperatures is caused by an increase in reactor thermal power.

Figure 18(d) shows the reactor power against time after the argon flow rate step. The maximum power is reached at about 130 seconds after the argon flow rate change. This maximum is about 14 percent greater than the initial design power. The final steady-state power is about 12 percent greater than the initial design value. The power behaves in the manner shown in figure 18(d) because of the temperature reactivity feedbacks.

The fuel temperatures in the three segments of the core are shown against time after the argon flow rate step in figures 18(e), (f), and (g). The temperature in each section decreases initially and then increases to a final steady-state value. In each section of the core, the final steady-state fuel temperature is slightly greater than the corresponding initial value.

The data just presented show that a change in argon flow rate has a significant effect on the transient and steady-state operating conditions in the primary flow loop.

The preceding sections described the transient behavior of the primary loop variables to three types of input step perturbations. These input perturbations were imposed with the system initially at its steady-state design operating level. In table IV, we have summarized some of the response data of the system for the three types of input step disturbances.

Of special significance in table IV is the reactor power settling time. With the system initially at its steady-state design point, the reactor power settling time for each reactivity step is about 275 seconds. However, at low-flow, off-design conditions, the reactor power settling times are considerably longer. For example, at a lithium flow rate equal to 10 percent of the design lithium flow rate, the reactor power settling time, following a step change in reactivity, is about 10 times the value shown in table IV, or about 2750 seconds.

In the section Steady-State Operating Characteristics, it was shown that the change in steady-state reactor power is directly proportional to the inserted reactivity. However, the transient peak change in reactor power is not proportional to the reactivity step change. Table IV shows that for a 5-cent reactivity step, the ratio of peak reactor power to final steady-state power is about 2.6. But for a 30-cent reactivity step, this ratio is about 4.5. Hence, the ratio of peak change to final steady-state change in reactor power increases with the reactivity step size.

Effect of Doppler Coefficient

The preceding results were based on a Doppler feedback coefficient which was calculated from equation (3). The Doppler coefficient given by equation (3) was estimated by the method described in reference 9. This Doppler coefficient is considered to be the best estimate at this time. However, until experimental verification is made, some uncertainty exists in the actual value of this coefficient. Because of this uncertainty, a study was made to examine the effect of the Doppler coefficient on the system response.

Three different values of Doppler coefficient were used: a negative value, a zero value, and a positive value. The equations used to calculate these Doppler coefficients and the magnitudes of these coefficients at the reactor design operating temperatures are listed in table V. The equation for the negative Doppler coefficient in table V is identical to equation (3).

We investigated the effect of these Doppler coefficients on the system response by inserting a step reactivity change into the system. The magnitude of the step change was 20 cents. And it was made at time zero with the system operating at its design point.

The time response of the system following this step in reactivity is shown in figure 19. The parameter in this figure is the Doppler coefficient.

The effect of Doppler coefficient on the reactor power response is given in figure 19(a). This figure shows reactor power against time after the 20-cent reactivity step. For the three Doppler coefficients, the time to reach peak power ranges from about 30 to 35 seconds. And the reactor power settling time for each of the three coefficients is about 275 seconds. The values of the peak power are about 224 percent, 208 percent, and 198 percent of design for the positive, zero, and negative Doppler coefficients, respectively. The difference in final steady-state power for positive and negative Doppler coefficients is about 9 percent.

Figures 19(b), (c), and (d) show the fuel temperatures in core segments 1, 2, and 3 against time with Doppler coefficient as a parameter. In each core segment, the peak fuel temperature for the positive Doppler coefficient is about 90° R (50 K) greater than the peak fuel temperature for the negative Doppler coefficient. And in each core segment, the final steady-state fuel temperature for the positive Doppler coefficient is about 65° R (36 K) greater than the final steady-state fuel temperature for the negative Doppler coefficient.

Figure 19(e) shows the lithium temperature rise across the core against time with Doppler coefficient as a parameter. The values of peak lithium temperature rise are about 215° R (119 K), 200° R (111 K), and 190° R (106 K) for the positive, zero, and negative Doppler coefficients, respectively. The final steady-state lithium temperatures for positive and negative Doppler coefficients differ by about 9° R (5 K).

The preceding paragraphs have shown the effect of negative, zero, and positive Doppler coefficients on the transient response of the system. In general, for the range of Doppler coefficients used, the system response was not significantly affected by the Doppler coefficient. The reason for this is that the reactivity feedbacks due to the lithium density δk_ρ and the core expansion δk_E have relatively large negative values, and therefore, they have a predominate effect on the system response. Consequently, even when the positive Doppler coefficient was used, the net feedback (which is the sum of δk_E, δk_ρ, and δk_D) remains significantly negative.

SUMMARY OF RESULTS

An investigation was made of the operation of the primary flow loop of a conceptual nuclear Brayton space powerplant. As a result of this investigation, the following were determined: (1) the effects of off-design operation on the steady-state reactor power and steady-state temperatures in the primary loop; (2) the transient response characteristics of the primary loop to step disturbances (forced perturbations) in reactivity, lithium flow rate, and inert-gas flow rate; and (3) the effect of the Doppler reactivity coefficient on the transient response of the system primary loop. The specific results obtained from this system investigation are as follows:

1. The steady-state power output of the reactor is a linear function of the inserted reactivity. A reactivity insertion of 10 cents causes a change of about 12 percent in the reactor steady-state power.

2. The flow rate of inert-gas in the power conversion loop has a significant effect on the reactor steady-state power. The inert-gas flow rate affects the rate of heat removal from the primary loop and, consequently, the temperatures in the loop. And because of the temperature reactivity feedbacks, the reactor power also changes. For this system, the reactor steady-state power was found to be proportional to the inert-gas flow rate. A 10 percent change in the inert-gas flow rate causes about a 9 percent change in the reactor steady-state power.

3. The flow rate of lithium in the primary loop has a small effect on the reactor steady-state power. With the system initially at its design operating point, a step increase of 15 percent in lithium flow rate causes the reactor steady-state power to increase by about 0.05 percent.

4. The transient response of the system following step changes in inserted reactivity, lithium flow rate, and inert-gas flow rate can be characterized at stable and highly damped.

With the system initially at its design operating point, a step increase of 30 cents in inserted reactivity results in a peak (or maximum) increase in reactor power of about

172 percent. The reactor power settling time corresponding to a 30-cent step increase in inserted reactivity is about 275 seconds.

5. The transient change in the reactor power and system temperatures following a step change in lithium flow rate is relatively small. The peak (or maximum) increase in reactor power resulting from a 15 percent increase in lithium flow rate is about 1.2 percent.

6. A step change in the inert-gas flow rate causes a significant transient change in the system conditions. With the system initially at its design operating point, a step increase of 15 percent in argon flow rate results in a peak transient increase in reactor power of about 17 percent.

7. The system response did not change appreciably for the different values of Doppler coefficient used in this investigation. Even when the Doppler reactivity coefficient was considered positive, the system response was stable and highly damped.

Lewis Research Center,
National Aeronautics and Space Administration,
Cleveland, Ohio, November 16, 1970,
120-27.

APPENDIX A - SYMBOLS

A	flow area, ft^2; m^2
A_m	log-mean area for heat conduction, ft^2; m^2
C_p	heat capacity, Btu/(lbm)(^oR); $(k_W)(sec)/(kg)(K)$
D	hydraulic diameter, ft; m
D_i	contribution to power from i^{th} group of delayed neutron precursors, Btu/sec; kW
d	outside diameter of tubes in heat-source heat exchanger, ft; m
f	fraction of total power generated in fuel segment
h	heat-transfer coefficient, Btu/(sec)(ft^2)(^oR); kW/(m^2)(K)
k	thermal conductivity, Btu/(ft)(sec)(^oR); kW/(m)(K)
δk	reactivity
δk_D	reactivity feedback due to Doppler effect
δk_E	reactivity feedback due to core expansion
δk_ρ	reactivity feedback due to lithium density change
L	length, ft; m
ℓ^*	prompt neutron generation time, sec
Nu	Nusselt number
Pe	Peclet number
Pr	Prandtl number
$\dot{Q}$	reactor power, Btu/sec; kW
Δr	incremental distance in radial direction, ft; m
Re	Reynolds number
S	heat-transfer surface area, ft^2; m^2
s	centerline-to-centerline distance between tubes in heat-source heat exchanger, ft; m
T	temperature, ^oR; K
ΔT	temperature increment, ^oR; K
$\overline{T}$	average temperature associated with segment of core or heat exchanger, ^oR; K
t	time, sec

V	volume, ft^3; m^3
ΔX	incremental distance in axial direction, ft; m
β	fraction of fission neutrons which are delayed
β_i	fraction of delayed fission neutrons belonging to i^{th} group
λ_i	decay constant of delayed neutron precursor in i^{th} group, sec^{-1}
ρ	density, lbm/ft^3; kg/m^3
$\dot{\omega}$	flow rate, lbm/sec; kg/sec

Subscripts:

av	average
c	core
F	fuel
g	argon gas
HX	heat exchanger
in	segment inlet
K	fuel cladding
L	liquid lithium
out	segment outlet
seg 1	segment 1
seg 2	segment 2
seg 3	segment 3
W	tube wall of heat exchanger
1	reactor inlet
2	reactor outlet
3	heat exchanger inlet
4	heat exchanger outlet

REFERENCES

1. Davison, Harry W.: Preliminary Analysis of Accidents in a Lithium-Cooled Space Nuclear Powerplant. NASA TM X-1937, 1970.

2. Thompson, T. J.; and Beckerley, J. G., eds.: Reactor Physics and Control. Vol. 1 of The Technology of Nuclear Reactor Safety. MIT Press, 1964.

3. Ash, Milton: Nuclear Reactor Kinetics. McGraw-Hill Book Co., Inc., 1965.

4. Barber, Clayton E.: A FORTRAN IV Two-Dimensional Discrete Angular Segmentation Transport Program. NASA TN D-3573, 1966.

5. Dwyer, O. E.: On the Transfer of Heat to Fluids Flowing Through Pipes, Annuli, and Parallel Plates. Nucl. Sci. Eng., vol. 17, no. 3, Nov. 1963, pp. 336-344.

6. Dwyer, O. E.: Recent Developments in Liquid-Metal Heat Transfer. At. Energy Rev., vol. 4, no. 1, 1966, pp. 3-92.

7. Kreith, Frank: Principles of Heat Transfer. International Textbook Co., 1958.

8. Weaver, Lynn E.: System Analysis of Nuclear Reactor Dynamics. Rowman and Littlefield, Inc., 1963.

9. Brehm, Richard L.: Estimates of Doppler Coefficients for In-Pile Thermionic Reactor Materials. Tech. Rep. 32-1077, Jet Propulsion Lab., California Inst. Tech. (NASA CR-85358), Oct. 1, 1967.

TABLE I. - DESIGN POINT OPERATING CONDITIONS

Reactor thermal power, $\dot{Q}$, MW thermal	2.17
Lithium temperature at reactor inlet, T_1, $^{o}R(K)$	2100(1167)
Lithium temperature at reactor outlet, T_2, $^{o}R(K)$	2200(1222)
Lithium flow rate, $\dot{\omega}_L$, lbm/sec (kg/sec)	20.70(9.39)
Argon temperature at heat exchanger inlet, T_3, $^{o}R(K)$	1560(867)
Argon temperature at heat exchanger outlet, T_4, $^{o}R(K)$	2060(1144)
Argon flow rate, $\dot{\omega}_g$, lbm/sec (kg/sec)	32.80(14.88)

TABLE II. - DECAY CONSTANTS AND YIELD FRACTIONS OF DELAYED NEUTRON PRECURSORS AND PROMPT NEUTRON GENERATION TIME[a] FOR FAST FISSION OF URANIUM 235

Delay group	Decay constant, λ_i, sec^{-1}	Yield fraction, β_i
1	3.8800	0.0001719
2	1.4000	.0008431
3	.3110	.0026910
4	.1160	.0012380
5	.0317	.0014020
6	.0127	.0002517
	Total	0.0065977

[a]Prompt neutron generation time $\ell^* = 4.0\times10^{-8}$ sec.

TABLE III. - DESIGN VALUES OF AVERAGE FUEL, CLAD, AND LITHIUM TEMPERATURES IN THE CORE AND VALUES OF FEEDBACK COEFFICIENTS AT THE DESIGN TEMPERATURES

Average fuel temperature, $T_{F,av}$, $^{o}R(K)$	2270(1262)
Average clad temperature, $T_{K,av}$, $^{o}R(K)$	2178(1210)
Average lithium temperature in core, $T_{L,av}$, $^{o}R(K)$	2174(1208)
Reactivity temperature coefficient due to Doppler, $d(\delta k_D)/dT$, $^{o}R^{-1}(K^{-1})$	$-1.038\times10^{-6}(-1.87\times10^{-6})$
Reactivity temperature coefficient due to core expansion, $d(\delta k_E)/dT$, $^{o}R^{-1}(K^{-1})$	$-5.69\times10^{-6}(-10.24\times10^{-6})$
Reactivity temperature coefficient due to lithium density, $d(\delta k_\rho/dT$, $^{o}R^{-1}(K^{-1})$	$-1.63\times10^{-6}(-2.93\times10^{-6})$

TABLE IV. - SUMMARY OF SYSTEM RESPONSE CHARACTERISTICS FOLLOWING STEP CHANGES IN REACTIVITY, LITHIUM FLOW RATE, AND ARGON FLOW RATE (SYSTEM INITIALLY AT ITS DESIGN OPERATING CONDITIONS)

Input disturbance	Magnitude of disturbance	Reactor power				Average fuel temperature of section 3, $^{o}R(K)$		Reactor power settling time, sec
		Peak change		Steady-state change		Peak change	Steady-state change	
		Percent	MW	Percent	MW			
Step increase in reactivity	5 cents	16.0	0.35	6.2	0.135	60 (33)	45 (25)	~ 275
Step increase in reactivity	10 cents	42.0	.92	12.0	.27	120 (67)	90 (50)	~ 275
Step increase in reactivity	20 cents	99.0	2.2	25.0	.54	250 (139)	185 (103)	~ 275
Step increase in reactivity	30 cents	172.0	3.7	38.0	.82	390 (217)	275 (153)	~ 275
Step increase in lithium flow rate	15 percent of design value	1.2	.026	.05	.0011	-8 (-4.5)	-4 (-2.2)	~ 120
Step increase in argon flow rate	15 percent of design value	17.0	.37	14.0	.30	19 (11)	9 (5)	~ 210

TABLE V. - DOPPLER COEFFICIENT EQUATIONS AND VALUES AT DESIGN OPERATING CONDITIONS

Type of Doppler coefficient	Doppler coefficient equation	Value of Doppler coefficient at design conditions	
		$^{o}R^{-1}$	K^{-1}
Negative	$\frac{d(\delta k_D)}{dT} = \frac{2.17\times10^{-4}}{T_{F,av}} - 6.465\times10^{-4}T_{K,av}^{-0.8}$	-1.038×10^{-6}	-1.87×10^{-6}
Zero	$\frac{d(\delta k_D)}{dT} = 0$	0	0
Positive	$\frac{d(\delta k_D)}{dT} = -\left(\frac{2.17\times10^{-4}}{T_{F,av}} - 6.465\times10^{-4}T_{K,av}^{-0.8}\right)$	1.038×10^{-6}	1.87×10^{-6}

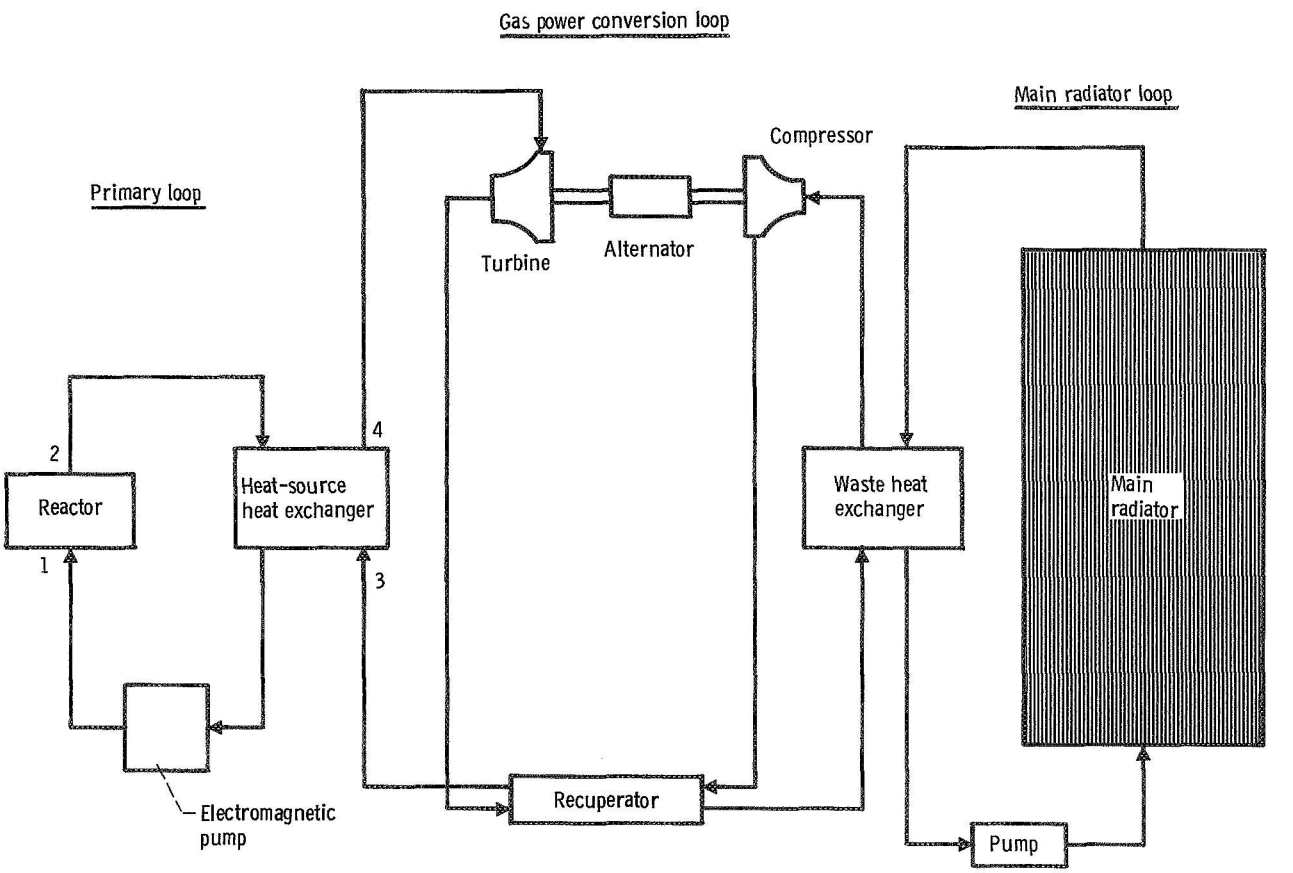

Figure 1. - Schematic diagram of conceptual nuclear Brayton space powerplant.

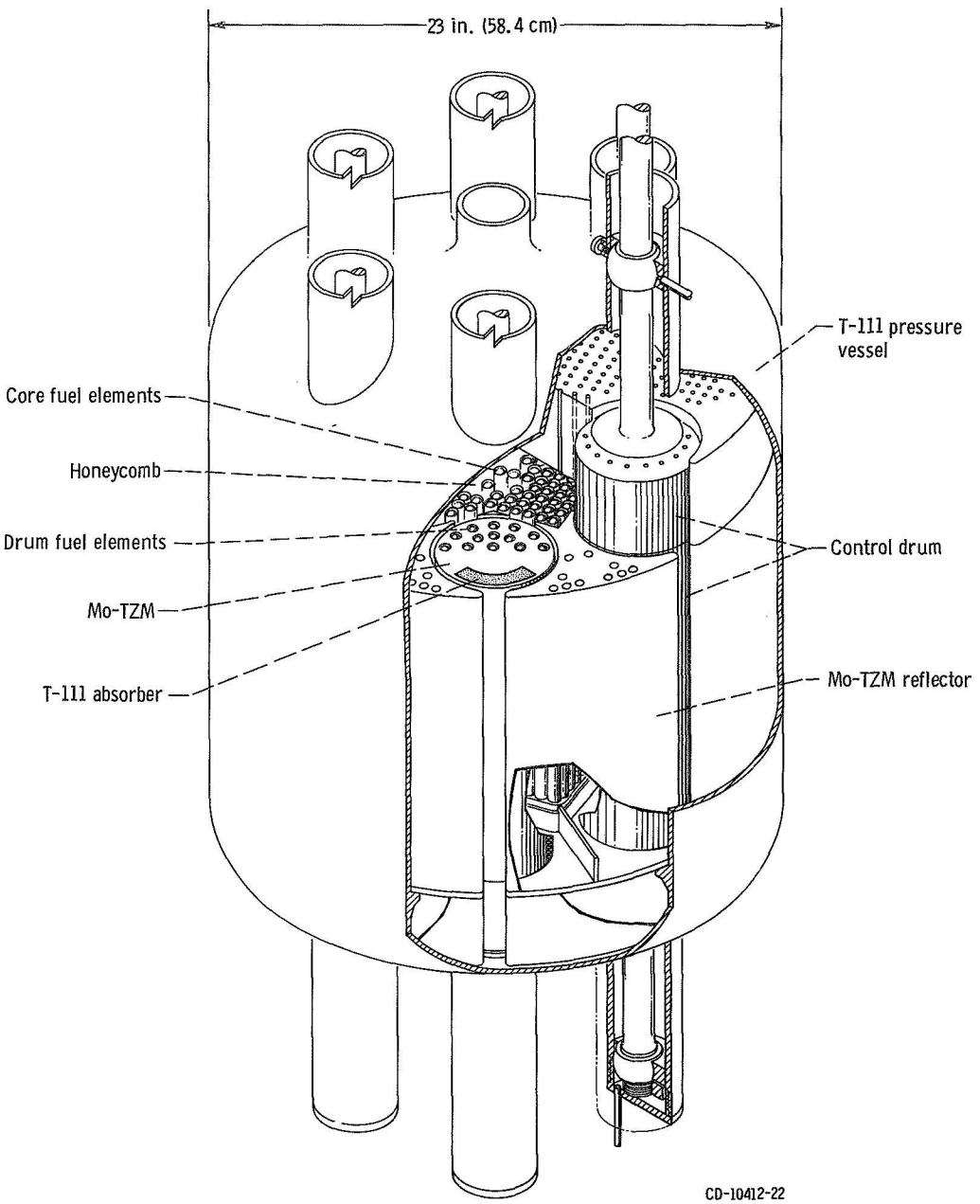

Figure 2. - Nuclear Brayton space power reactor.

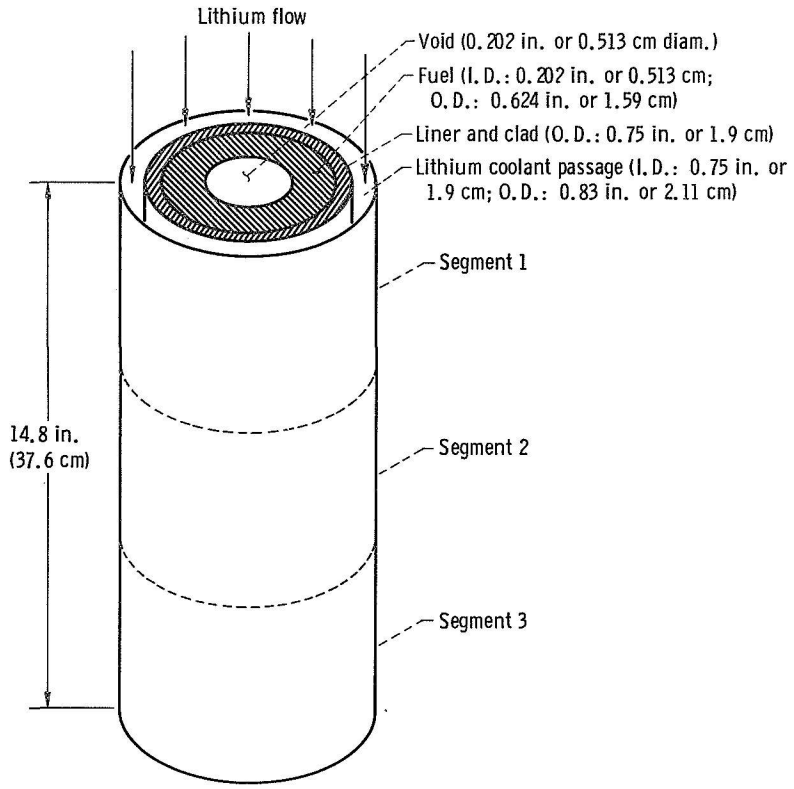

Figure 3. - Single fuel pin model of reactor core (not to scale).

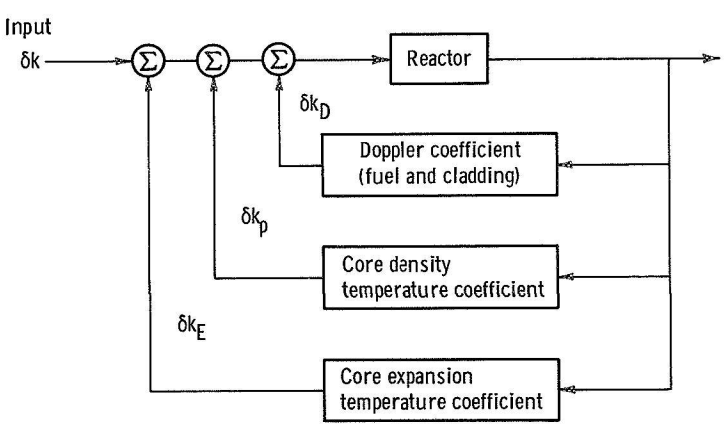

Figure 4. - Block diagram of reactor with three-path feedback.

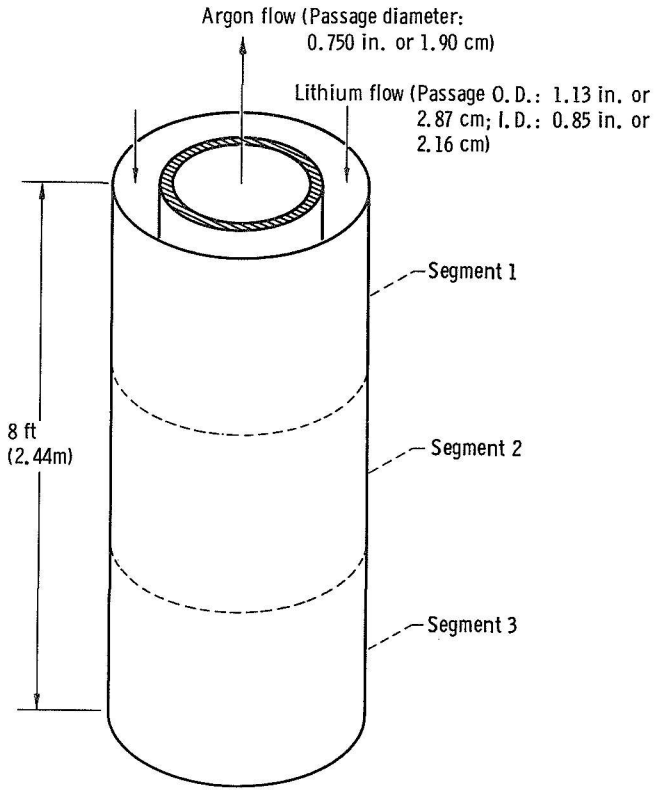

Figure 5. - Single tube model of shell-and-tube heat exchanger (not to scale).

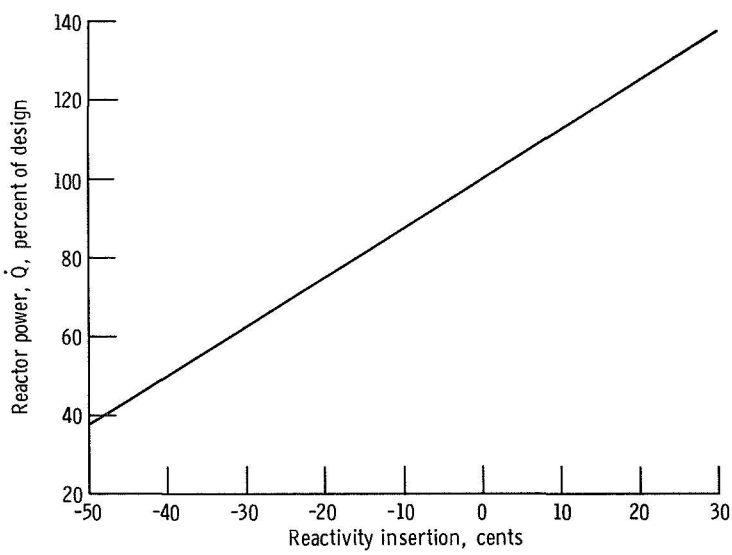

Figure 6. - Steady-state reactor power as a function of reactivity insertion with lithium and argon flow rates at their respective design values.

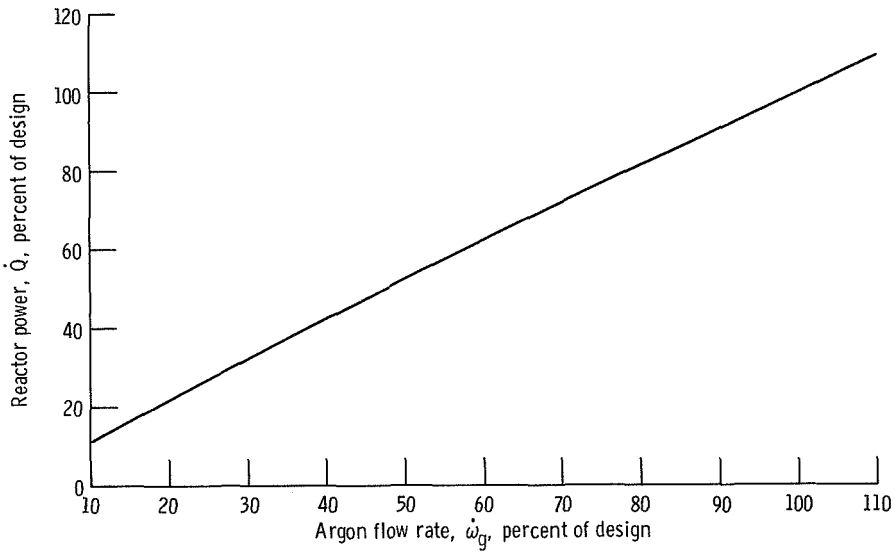

Figure 7. - Steady-state reactor power as a function of argon flow rate with lithium flow rate at its design value.

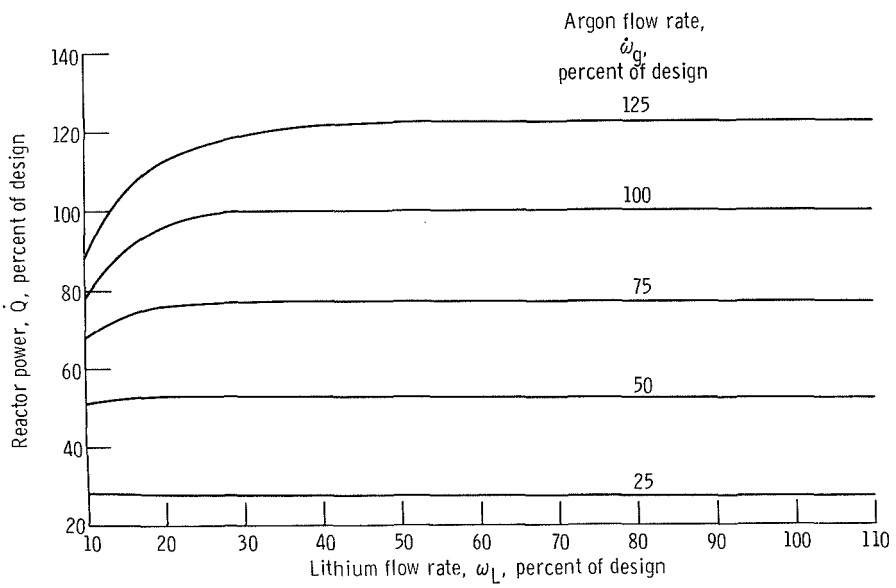

Figure 8. - Steady-state reactor power as a function of lithium flow rate with argon flow rate as a parameter.

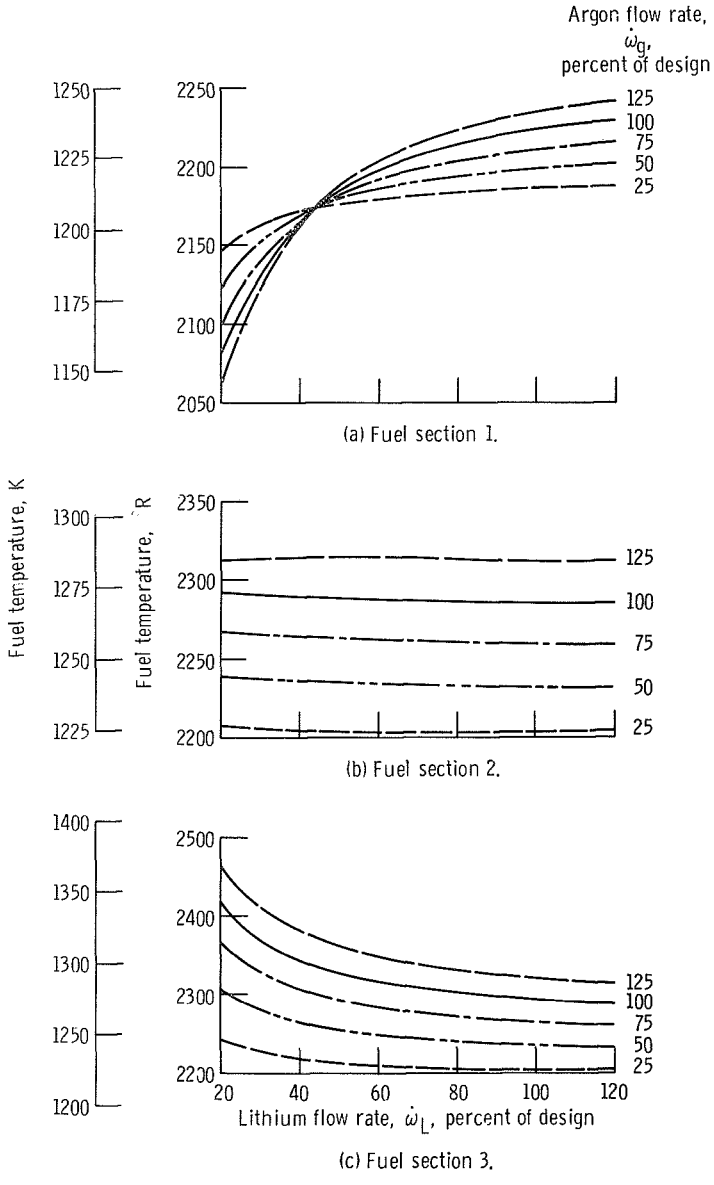

Figure 9. - Steady-state average temperature of fuel segments 1, 2, and 3 against lithium flow rate with argon flow rate as a parameter.

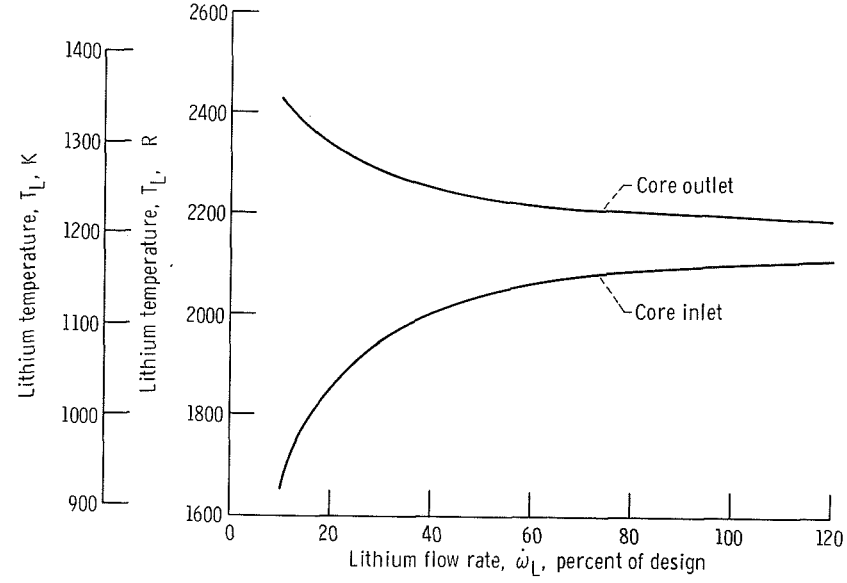

Figure 10. - Steady-state lithium temperature at core inlet and core outlet as a function of lithium flow rate with argon flow rate at design value.

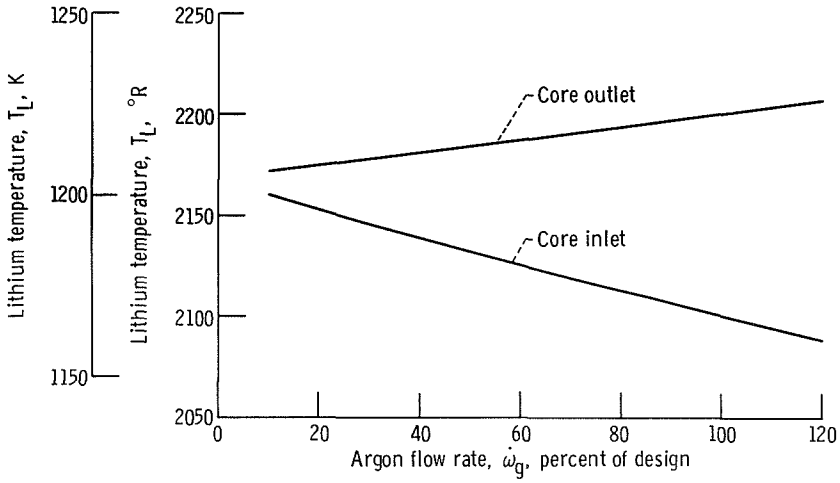

Figure 11. - Steady-state lithium temperature at core inlet and core outlet as a function of argon flow rate with lithium flow rate at its design value.

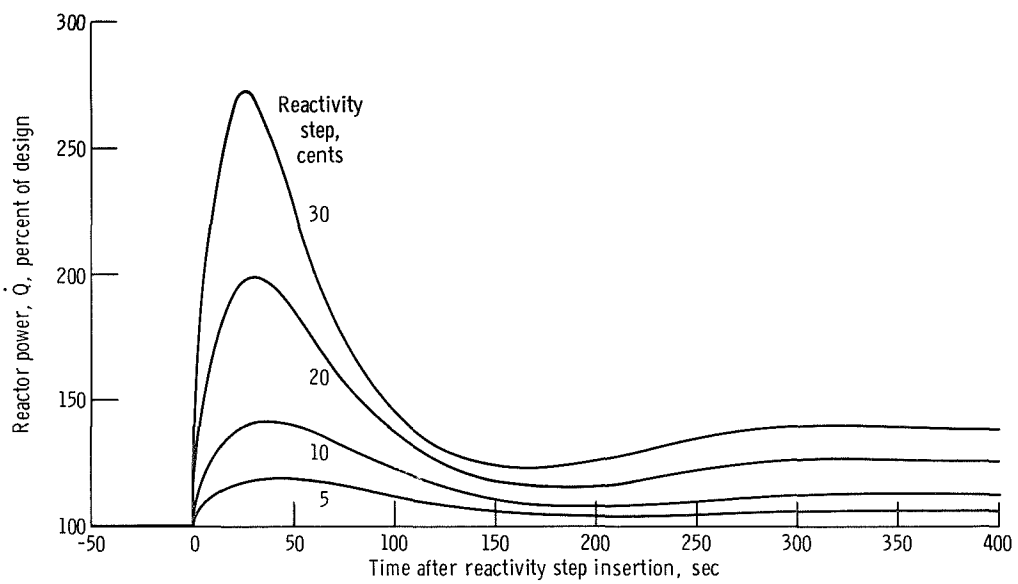

Figure 12. - Reactor power against time for reactivity step insertions of 5, 10, 20, and 30 cents.

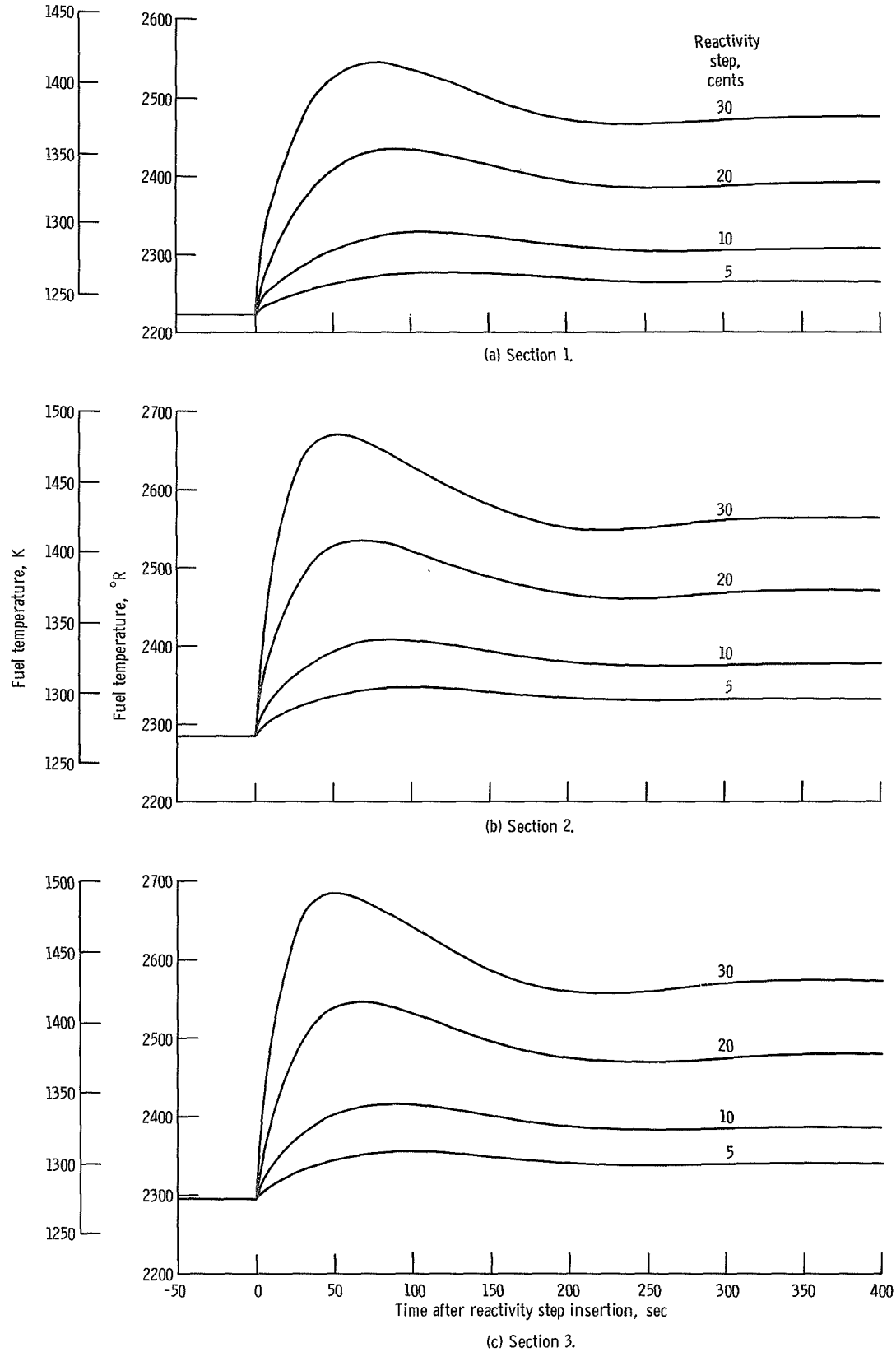

Figure 13. - Average fuel temperature of sections 1, 2, and 3 against time for reactivity step insertions of 5, 10, 20, and 30 cents.

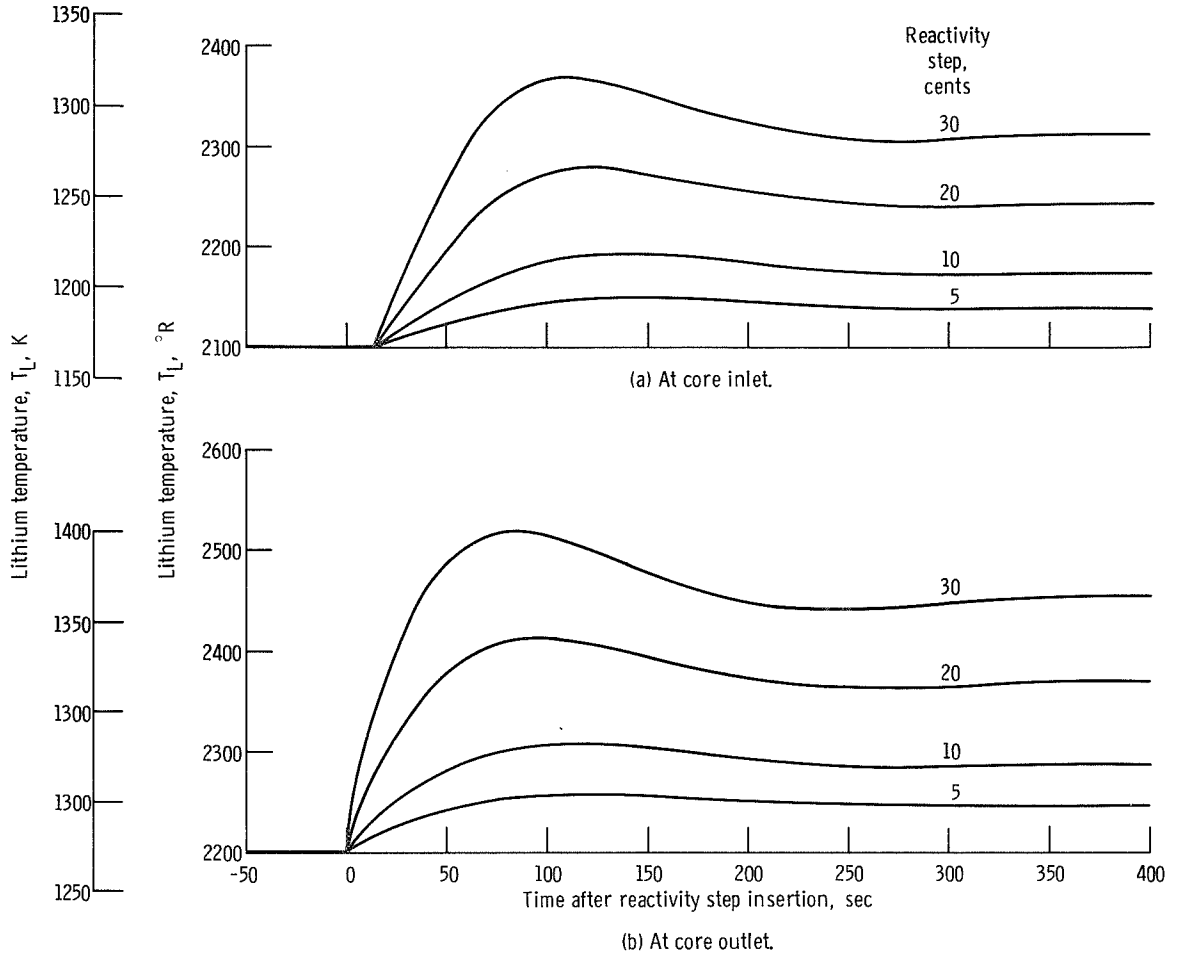

Figure 14. - Lithium temperature at core inlet and core outlet against time for reactivity step insertions of 5, 10, 20, and 30 cents.

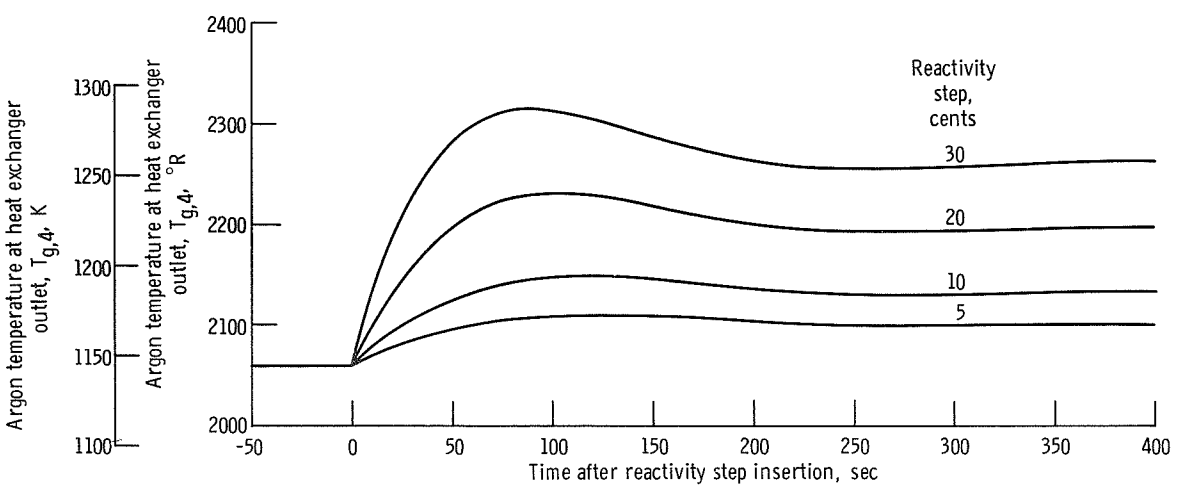

Figure 15. - Argon temperature at heat exchanger outlet against time for reactivity step insertions of 5, 10, 20, and 30 cents.

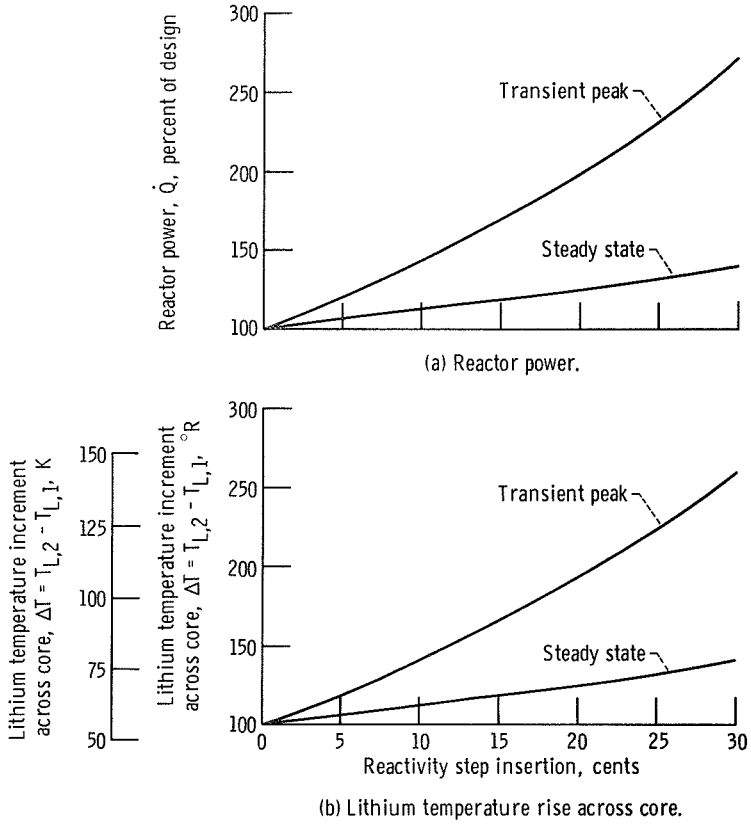

(a) Reactor power.

(b) Lithium temperature rise across core.

Figure 16. - Peak and steady-state values of reactor power, lithium temperature rise across core, and fuel temperatures against reactivity step insertion.

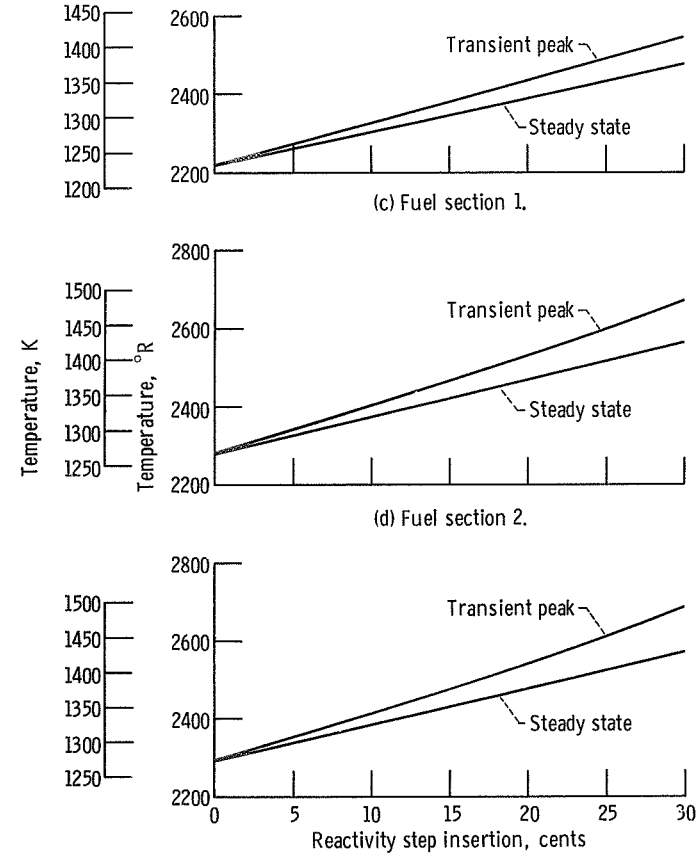

(c) Fuel section 1.

(d) Fuel section 2.

(e) Fuel section 3.

Figure 16. - Concluded.

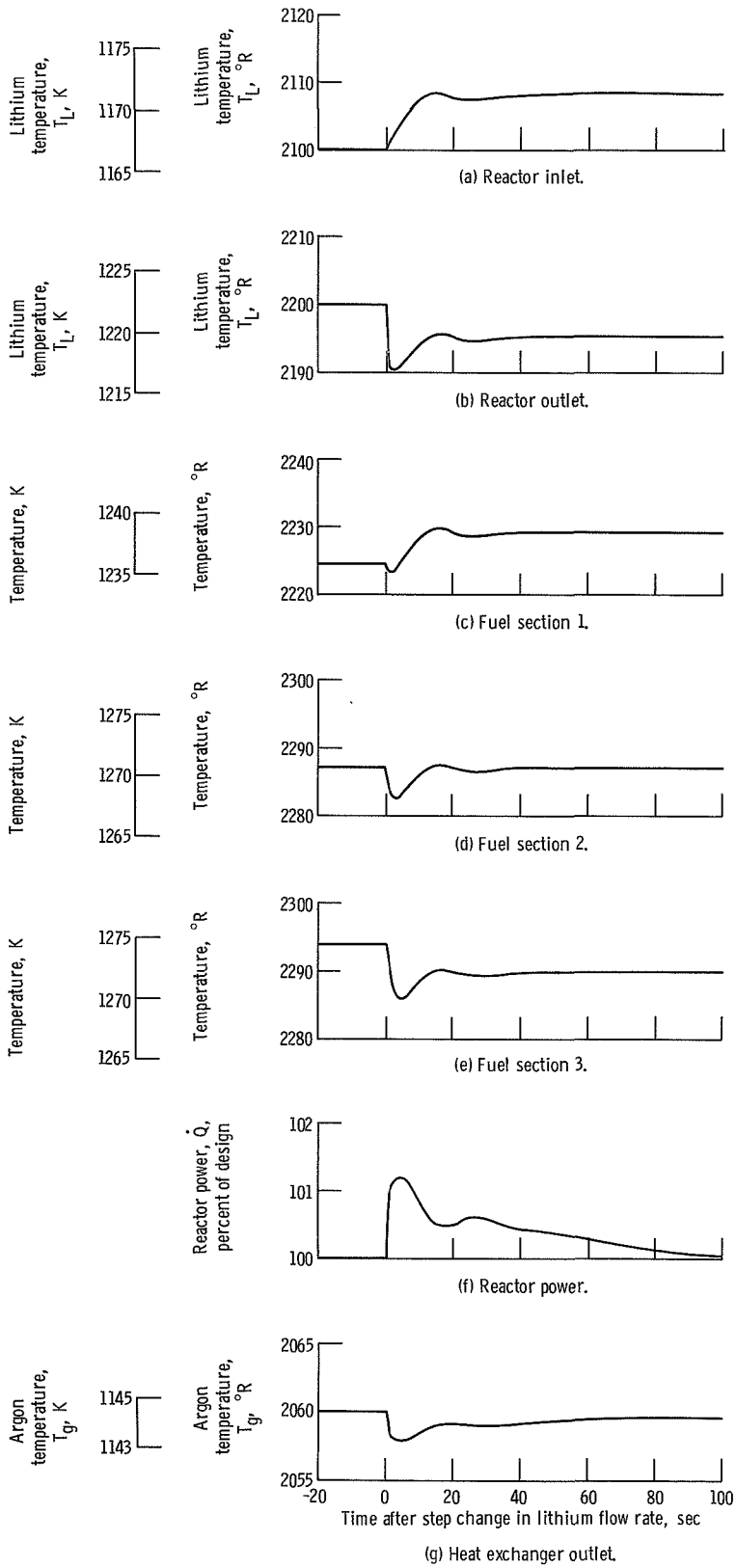

Figure 17. - Transient response of lithium temperatures, fuel temperatures, reactor power, and argon temperature to 15 percent step increase in lithium flow rate.

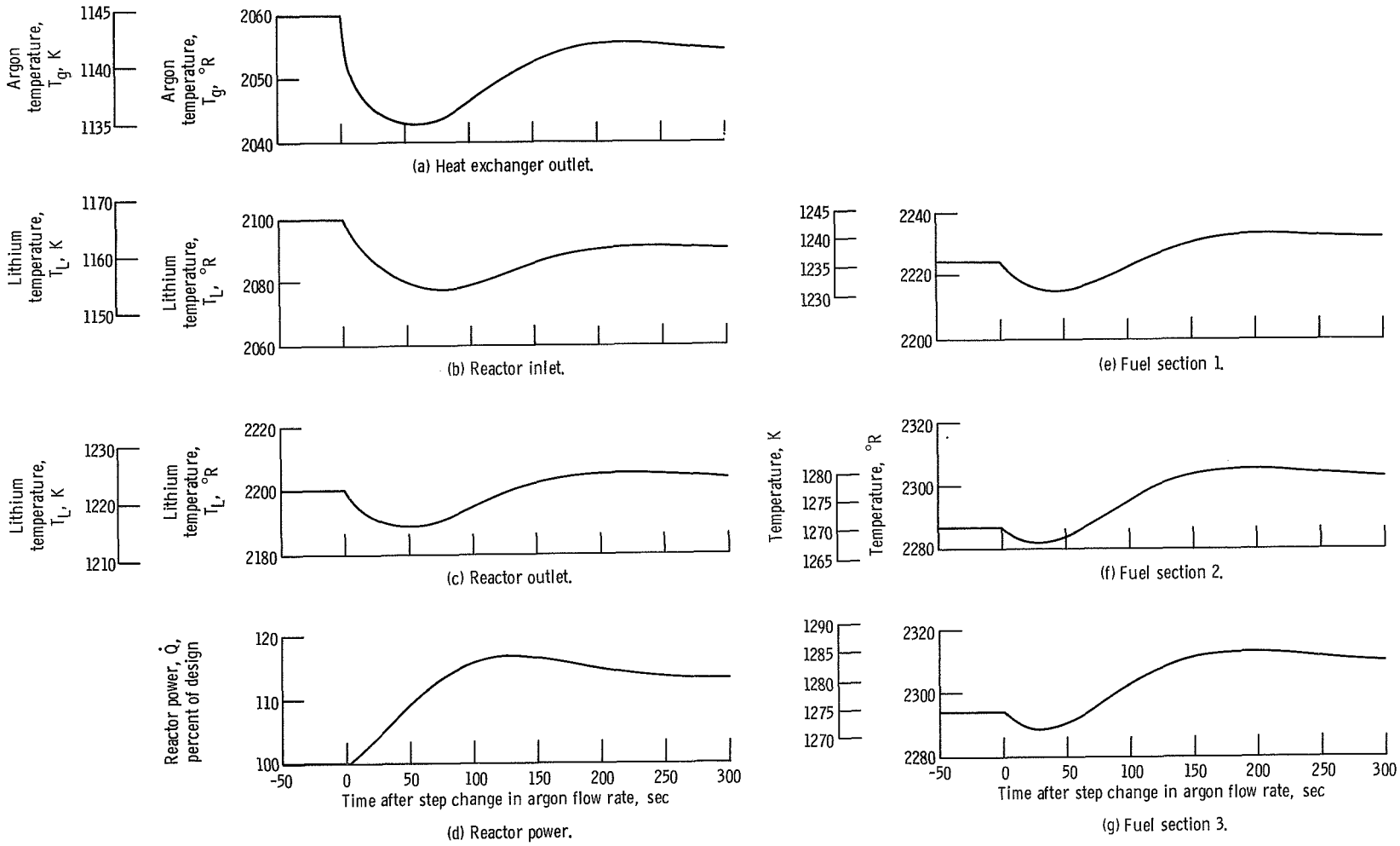

Figure 18. - Transient response of argon temperature, lithium temperatures, reactor power, and fuel temperatures to 15 percent step increase in argon flow rate.

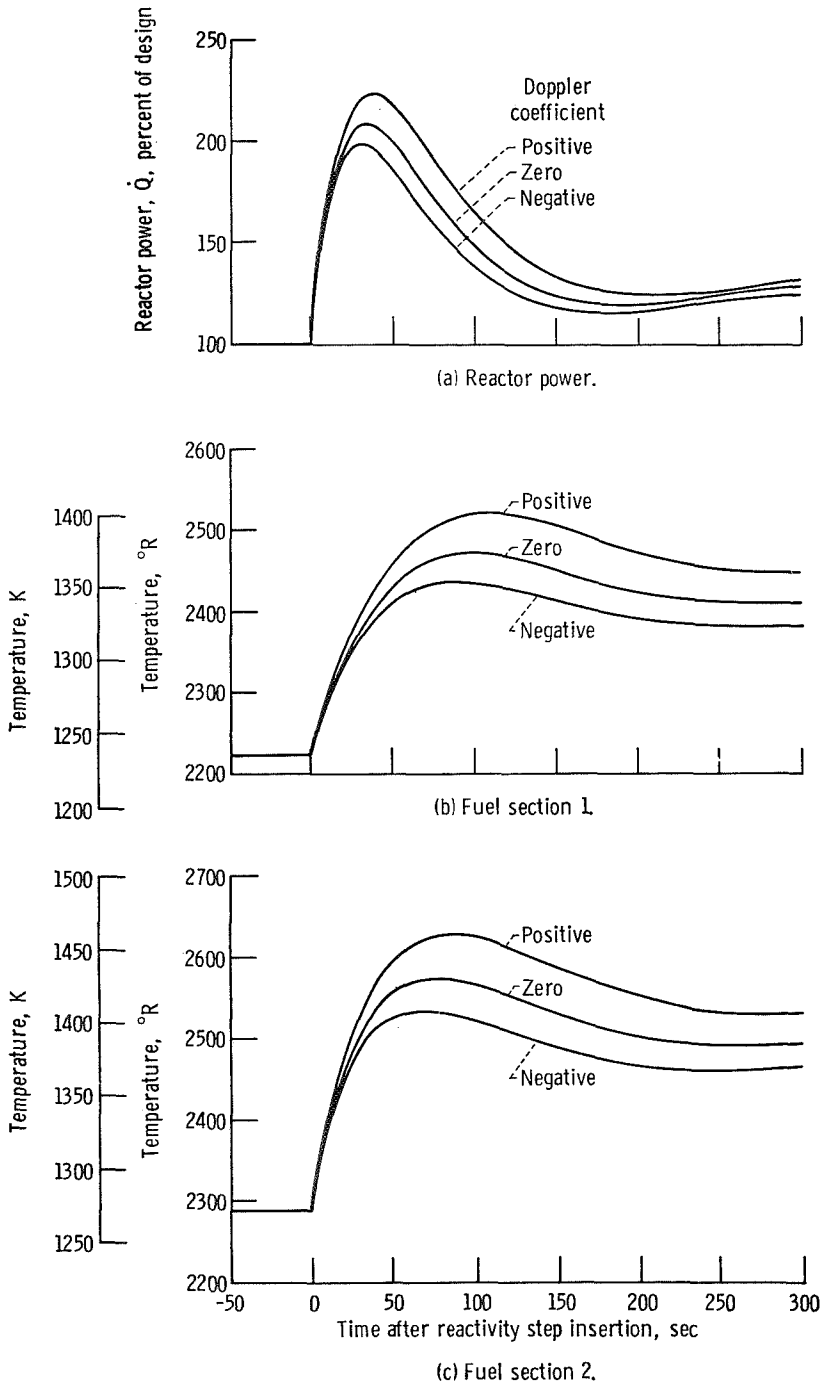

Figure 19. - Transient response of reactor power, fuel temperatures, and lithium temperature increment across core to 20-cent step change in reactivity with Doppler feedback coefficient as a parameter.

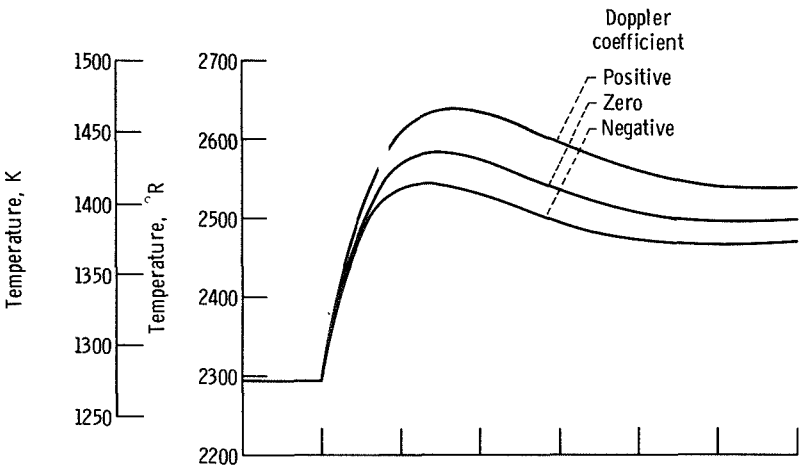

(d) Fuel section 3.

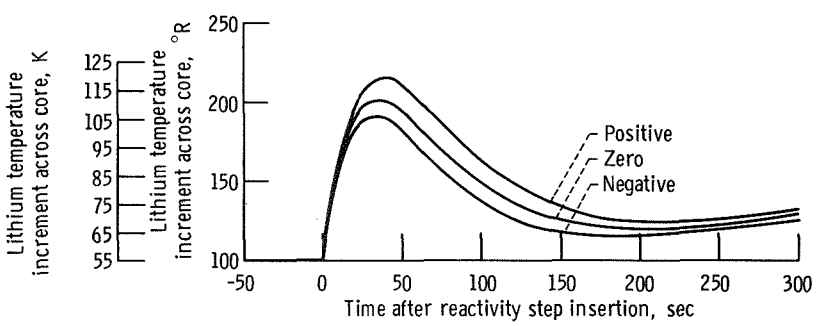

(e) Lithium temperature rise across core.

Figure 19. - Concluded.

NASA-Langley, 1971 —— 22 E-5903

NATIONAL AERONAUTICS AND SPACE ADMINISTRATION
WASHINGTON, D.C. 20546

OFFICIAL BUSINESS

FIRST CLASS MAIL

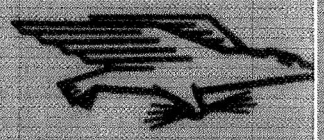

POSTAGE AND FEES PAID
NATIONAL AERONAUTICS AN
SPACE ADMINISTRATION

POSTMASTER: If Undeliverable (Section 158 Postal Manual) Do Not Retur

"The aeronautical and space activities of the United States shall be conducted so as to contribute . . . to the expansion of human knowledge of phenomena in the atmosphere and space. The Administration shall provide for the widest practicable and appropriate dissemination of information concerning its activities and the results thereof."

—NATIONAL AERONAUTICS AND SPACE ACT OF 1958

NASA SCIENTIFIC AND TECHNICAL PUBLICATIONS

TECHNICAL REPORTS: Scientific and technical information considered important, complete, and a lasting contribution to existing knowledge.

TECHNICAL NOTES: Information less broad in scope but nevertheless of importance as a contribution to existing knowledge.

TECHNICAL MEMORANDUMS: Information receiving limited distribution because of preliminary data, security classification, or other reasons.

CONTRACTOR REPORTS: Scientific and technical information generated under a NASA contract or grant and considered an important contribution to existing knowledge.

TECHNICAL TRANSLATIONS: Information published in a foreign language considered to merit NASA distribution in English.

SPECIAL PUBLICATIONS: Information derived from or of value to NASA activities. Publications include conference proceedings, monographs, data compilations, handbooks, sourcebooks, and special bibliographies.

TECHNOLOGY UTILIZATION PUBLICATIONS: Information on technology used by NASA that may be of particular interest in commercial and other non-aerospace applications. Publications include Tech Briefs, Technology Utilization Reports and Technology Surveys.

Details on the availability of these publications may be obtained from:

SCIENTIFIC AND TECHNICAL INFORMATION OFFICE

NATIONAL AERONAUTICS AND SPACE ADMINISTRATION

Washington, D.C. 20546